Available online at www.sciencedirect.com
ScienceDirect
International Journal of Heat and Mass Transfer 51 (2008) 1017–1023
International Journal of HEAT and MASS TRANSFER
www.elsevier.com/locate/ijhmt

Determination of thermal contact resistance from transient temperature measurements

C. Fieberg, R. Kneer *

Lehrstuhl für Wärme- und Stoffübertragung, Rheinisch-Westfälische Technische Hochschule Aachen, D-52056 Aachen, Germany

Received 4 December 2006
Available online 5 July 2007

Abstract

The temperature distribution in combustion engine components is highly influenced by thermal contact resistance. For the prediction and optimisation of the thermal behaviour of modern combustion engines knowledge about the contact heat transfer is crucial.

Available correlations to predict the contact resistance are simplifications of the real geometric conditions and only tested for moderate pressures up to 7 MPa. Typical combustion engine applications include contact pressures up to 250 MPa.

The experimental approach presented here to derive the thermal contact resistance in terms of contact heat transfer coefficients for high temperature and high pressure conditions is based on transient infrared temperature measurements. Two bodies initially at two different temperatures are brought in contact and the surface temperature histories are recorded with a high-speed infrared camera. The contact heat flux is calculated by solving the related inverse problem. From the contact heat flux and from the measured temperature jump at the interface the contact heat transfer coefficient is calculated.

The inverse method used for the calculation of the heat flux is based on the analytical solution for a semi-infinite body and a step response to a Neumann boundary condition. This method provides an algorithm that is used in a sequential manner. The use of "future" temperature data greatly improve the stability of the governing equations and reduce the sensitivity to measurement errors.

Keywords: Thermal contact resistance; Inverse problem; Infrared thermography

1. Introduction

Thermal contact resistance is present at almost every contact between two surfaces with a technical roughness. There is a broad variety of applications which have been investigated for more than 50 years. An early calculation of the actual contact heat transfer coefficient was presented by Fenech and Rosenhow [5]. A first model considering elastic and plastic deformation of the surface peaks was proposed by Mikić [8]. Since then numerous authors have developed contact models for special applications, but only few of them considered high loads and high temperatures. Therefore, validated models exist only for contact pressures up to 7 MPa. With these models a reliable design and the prediction of contact resistances in combustion engines with temperatures up to 900 K and contact pressures of more than 200 MPa turn out to be rather difficult.

The most common way for measurement of contact conductance is the usage of steady-state experiments. Here, two bodies in contact are heated and cooled at their ends, respectively. The temperature distribution of these bodies in an evacuated environment is recorded by means of thermocouples inside the bodies. The linear temperature profile yields the constant gradient and the temperature jump at the interface by extrapolation. With these data the contact heat transfer coefficient is calculated following Eq. (1). The principle set up of such experiments is illustrated in Fig. 1.

$$h_c = \frac{\dot{q}''_c}{\Delta T} \tag{1}$$

* Corresponding author.
E-mail address: kneer@wsa.rwth-aachen.de (R. Kneer).

0017-9310/$ - see front matter © 2007 Elsevier Ltd. All rights reserved.
doi:10.1016/j.ijheatmasstransfer.2007.05.004

Nomenclature

H	hardness, MPa
h	heat transfer coefficient, W/m^2 K
k	thermal conductivity, W/m K
l	characteristic length, m
p	pressure, MPa
$\dot{q}$	heat flux, W
$\dot{q}''$	heat flux, W/m^2 K
T	temperature, °C
t	time, s
x	space variable, m

Greek symbols

α	thermal diffusivity, m^2/s
ΔT	temperature jump, K
ε	emissivity, –
Φ	step response to unit heat flux, m^2 K/W
$\tan\phi$	surface slope parameter, –
σ	surface roughness, μm

Dimensionless numbers

Bi	Biot number, hl/k
Fo	Fourier number, $\alpha t/x^2$

Subscripts

amb	ambient
c	contact
M	final time step
m	at time step, m
meas	measured
0	initial

A severe drawback of this method of investigation is the long waiting period of up to 8 h [7] to settle in a steady-state condition of the contact bodies. Furthermore, temperature measurements with thermocouples are an invasive method which modifies the thermal behaviour of the bodies and thus results in inaccurate results.

The infrared thermography is a new method to derive contact heat transfer coefficients from experimental investigations. With non-invasive and transient measurements of the temperature history of two attached bodies the contact resistance can be calculated by solving the related inverse problem. Le Niliot and Gallet [9] reconstructed the boundary wall heat flux using thermographic temperature measurements of the opposed wall and suggested this method to calculate contact heat transfer coefficients.

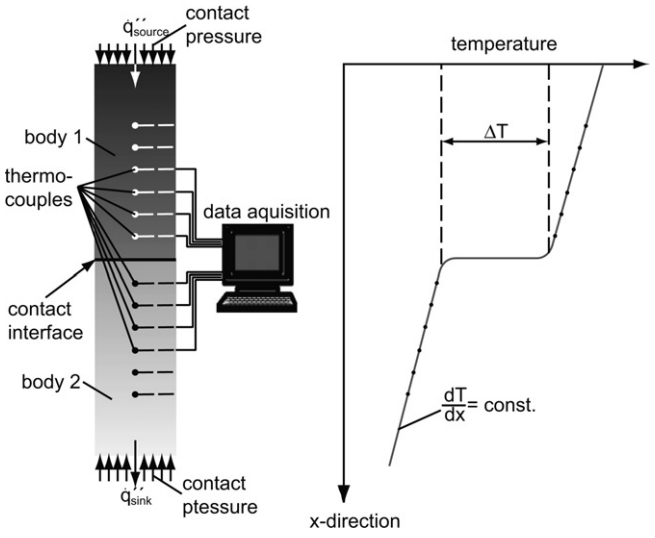

Fig. 1. Experimental set up for steady-state contact conductance investigations.

The present work demonstrates the capability of inverse methods to calculate contact heat transfer coefficients from transient temperature measurements with high pressure loads.

2. Experiments

The measurement of thermal contact resistance can be realised by two different methods. The direct and steady-state method as depicted in Fig. 1 measures the linear temperature profile in two bodies and gains the gradients and thus the heat flux following Fourier's law. To overcome the above mentioned restrictions of this method non-invasive temperature measurements with thermographic techniques are applied. One example is the "flash method" [10], where a short heat pulse by a spark light is imposed on one side of the material and the temperature response is recorded. From the normalised temperature data and the known solution of the partial differential equation for a pulse response the thermo-physical properties are evaluated. In case of two materials, the interstitial contact resistance can be calculated as a parameter. To solve this problem the solution of the related inverse problems is necessary [2]. Due to the experimental set up only joints without a load (welded joints, soldered joints) can be investigated. To gain knowledge about pressed joints the following variation of this thermographic method is introduced.

2.1. Experimental set up

The investigations presented in this work are focused on the contact conductance of materials applied in combustion engines. The materials selected are steel from the cylinder liner and Al-alloys from the piston. The test rig is a modified material testing system with a hydraulic driven

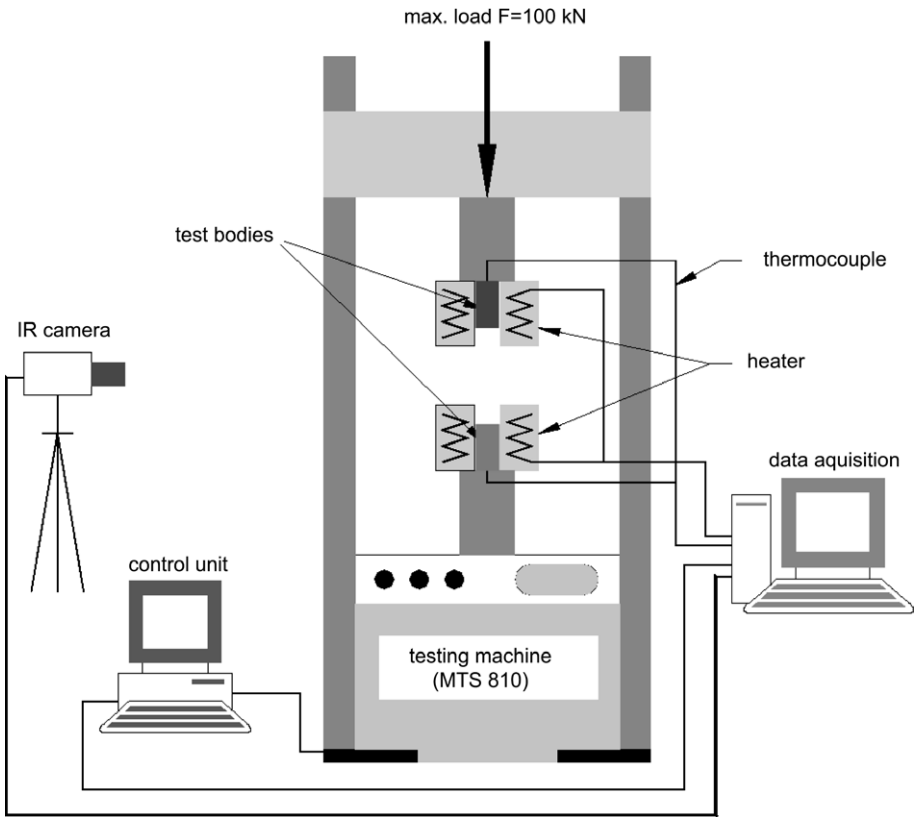

Fig. 2. Experimental set up for transient contact conductance investigations.

piston, Fig. 2. Two bodies are separately heated to different initial temperatures. The maximum temperature examined here is $T_{max} = 280$ °C. Once the bodies reach their initial temperature values, the two samples are brought into contact and pressed together to contact pressures up to 85 MPa. Higher pressures would be possible, but are not included in this work. The temperature change and thus the effect of the heat flux from the hot body to the colder one is recorded with a high-speed infrared camera. The two-dimensional temperature history of the body surfaces are the input for the evaluation of the inverse problem. The dimensions of the bodies and the thermal insulation yield a small Biot number ($Bi < 0.02$). Thus, the problem is one-dimensional and due to the very short contact times the temperature field in the bodies is assumed to be the one of a semi-infinite body.

2.2. Infrared thermography

The time dependent temperature distribution of the two bodies in contact is recorded with a long wave infrared camera which detects radiation in a wave length band from 7.7 to 9.5 μm. This wave length band is well suited for temperature measurements from 20 °C upwards, e.g., the maximum intensity emitted by a black body with 25 °C coincides just with this wave length interval, see Fig. 3. To avoid the influence of the surrounding radiation the

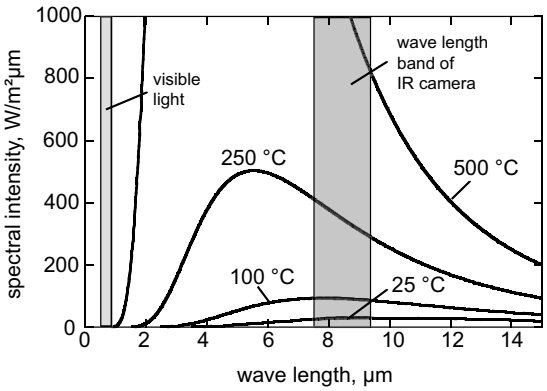

Fig. 3. Spectral intensity of a black body.

bodies have a high emissivity ($\varepsilon = 0.95$) due to a thin layer of black paint.

To minimise the errors while solving the inverse problem, it is crucial to measure the temperature adjacent to the contact line. Therefore, a microscope optic is used with a resolution of 13 μm/pixel which is very close to the diffraction resolution limit for this wave length band. With a frame size of 60×80 pixel (780×1040 μm) the frame rate used in the experiments is 2500 Hz. The results from the contact conductance experiments are the time dependent temperature data of the front side of the two bodies. This is the input data for solving the inverse problem.

3. Inverse heat conduction problems (IHCP)

The heat transfer coefficient at the contact interface is not measurable directly. It has to be calculated by an inverse method using the temperature information at a certain point in the spatial domain. In principle, the "cause", i.e., the heat flux, is calculated from the "effect", i.e., the temperature field. The mathematical procedure yields a unique but unstable solution. Thus, small noise in the temperature data can cause strong disturbances in the calculated heat flux.

In case of a one-dimensional problem, the partial differential equation with the boundary and initial conditions considering constant properties can be written as

$$\begin{aligned} &\frac{\partial T}{\partial t} = \alpha \frac{\partial^2 T}{\partial x^2} \quad T(x, t=0) = T_0 \\ &\dot{q}''_c = -k \left.\frac{\partial T}{\partial x}\right|_{x=0} \quad \left.\frac{\partial T}{\partial x}\right|_{x\to\infty} = 0 \end{aligned} \tag{2}$$

Although the bodies are bounded, contact time is too short for the heat flux to reach the far end of the bodies and thus the bodies can be treated as being semi-infinite.

To calculate the contact heat transfer coefficient h_c from Eq. (1) the heat flux across the contact area has to be calculated. Here, the sequential estimation introduced by Beck et al. [3] is used, where the heat flux is estimated stepwise including several future time steps ($r = 6$) to consider the continuous behaviour of the heat flux. The algorithm is displayed in Eq. (3).

$$\dot{q}''_c(x=0, t_m) = \frac{\sum_{i=1}^{r} (T_{\mathrm{meas},m+i-1} - \widehat{T}_{m+1-1}) \Phi_i(x = x_1, t_i)}{\sum_{i=1}^{r} \Phi_i^2(x = x_1, t_i)} \tag{3}$$

with the step response to a unit heat flux jump for a semi-infinite body [4]

$$\Phi(x,t) = \frac{x}{k}\sqrt{\frac{4\alpha t}{\pi}}\left(\frac{1}{\sqrt{\pi}}\exp\left(-\frac{1}{Fo}\right) - \frac{1}{\sqrt{4Fo}}\operatorname{erfc}\left(\frac{1}{\sqrt{4Fo}}\right)\right) \tag{4}$$

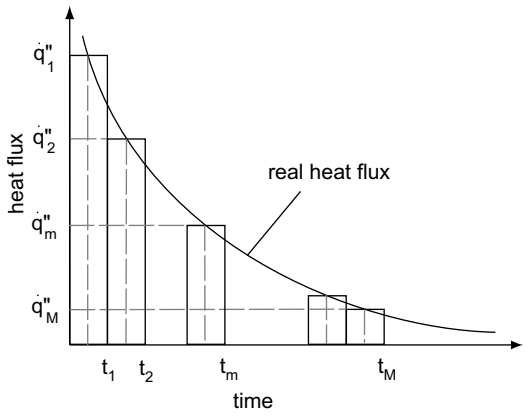

Fig. 4. Reconstruction of the boundary heat flux by superposition.

Eq. (4) consists only of physical constants and variables of space and time. Thus, it needs only be calculated once at the beginning of the procedure. Eq. (3) results from optimising the least square difference between the measured and calculated temperature of each time step based on the step response Φ. Fig. 4 illustrates the approximation of the contact heat flux by the superposition principle.

4. Results

The contact heat transfer coefficients are calculated from the measured temperature distribution in the bodies and the calculated heat flux at the interface. They are derived by Eq. (1) where the temperature difference ΔT is not measured exactly at the interface, but 50–100 μm adjacent to the contact. The temperature data at the interface is not usable because of a high noise level due to the deformation of the bodies. The difference between the actual temperature jump and the measured temperatures is supposed to be negligible.

This study focuses on the influence of the initial temperature of the bodies to the contact resistance and the pressure dependent contact heat transfer coefficient in a range from $p = 7$–85 MPa. The materials tested are steel and steel–aluminum alloy combinations. Both materials are common and widely used in industrial applications. The aluminum is much softer than the steel and will be deformed by the steel asperities at the contact interface. This should increase the heat transfer coefficient compared to a steel–steel combination.

The second focus is laid on the temperature dependency of the contact resistance. The thermo-physical properties and the material constants such as Young's modulus are a function of the body temperature and thus may influence the contact conductance. To examine the influence three different initial temperature conditions from 60/80 °C up to 260/280 °C are tested.

4.1. Data acquisition and post processing

The infrared camera records the two-dimensional temperature distribution adjacent to the contact interface. Fig. 5 gives an idea of the recorded images for different times.

The temperature distribution is one-dimensional due to a small Biot number ($Bi = hl/k \ll 1$). To reduce measurement noise, a horizontal line in the IR images is averaged and used as the input temperature for the IHCP algorithm. The resulting temperatures of one spot in each body versus time are presented in Fig. 6. From the temperature profile the contact heat flux is calculated by Eq. (3) to obtain the contact heat transfer coefficient (Eq. (1)) with the temperature jump of the two bodies from Fig. 6. The resulting contact heat transfer coefficient versus time is presented in Fig. 7. The heat transfer coefficient at the contact increases rapidly to a level of 14,500 W/m^2 K at $t = 0.4$ from which a much slower increase occurs. This second increase is an

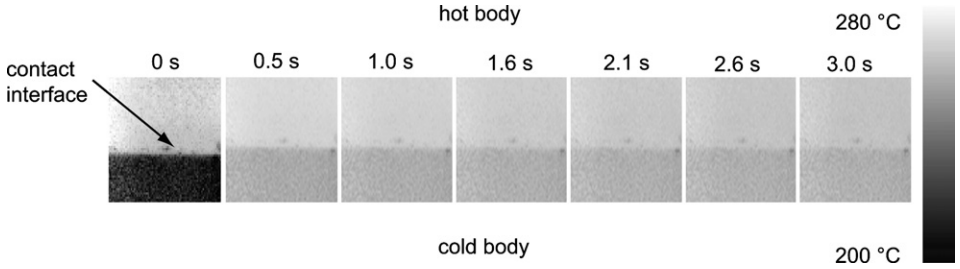

Fig. 5. IR images for different time steps, material: steel.

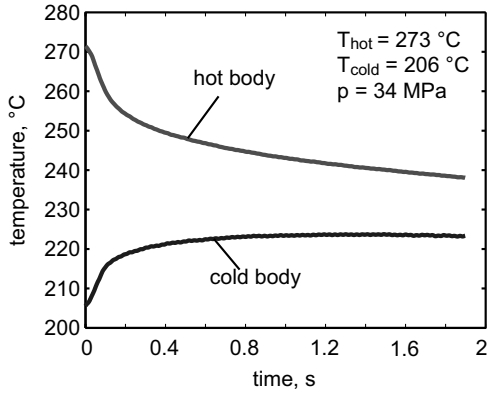

Fig. 6. Temperature of two points 52 μm from the contact line.

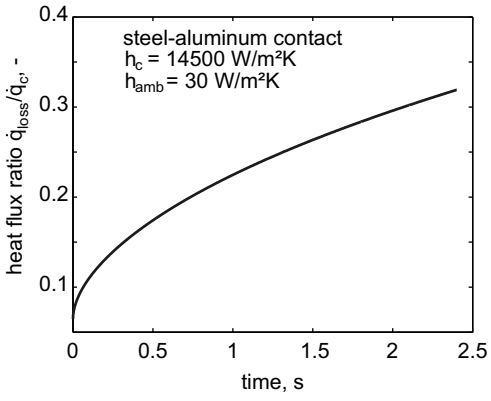

Fig. 8. Ratio of heat loss to ambient over contact heat flux.

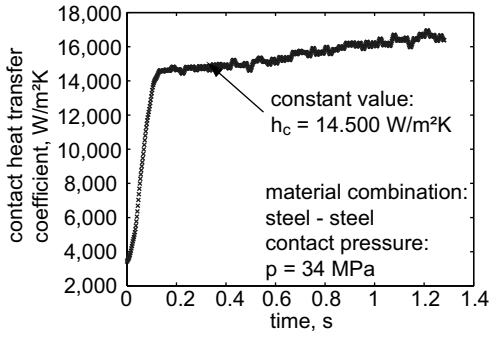

Fig. 7. Calculated contact heat transfer coefficient from measured temperature data.

artificial one due to the small temperature gradients shortly after the contact. Furthermore, the temperature difference between the two measured lines becomes smaller during the contact and leads to an increasing error in the temperature jump. Both effects influence the algorithm of the inverse problem solver and result in the artificial increase of the contact heat transfer coefficient. The further increase is not considered in the calculation of the heat transfer coefficient and thus generates no further errors as the short time period of $t = 0.4$ s is sufficient for the system to reach the steady-state value. Both bodies are cooled by convective and radiative losses to the ambient. In the calculation of the heat transfer coefficient these additional losses have an increasing influence. A comparison between the contact heat flux and the convective and radiative heat losses based on a Finite-Element calculation shows that the contact heat flux is only one order of magnitude larger than radiation and convection losses. It decreases fast while the heat flux to the ambient is almost constant, see Fig. 8. In the interesting time period just after contact, the error due to the convective losses is about 13%.

4.2. Contact heat transfer coefficients for different materials and contact pressures

The material combination of steel and aluminum is tested experimentally for contact pressures up to $p = 85$ MPa. Existing contact models such as the Mikić model [8] allow only the prediction of contact heat transfer coefficients for low contact pressures up to $p = 7$ MPa. This is the minimum pressure for the experimental set up presented here. Thus, a comparison with models from literature is only possible from this threshold on. The following equations show the correlations for the material combination for steel and aluminum for plastic deformation of the contact surface (Eq. (5a)) and plastic deformation with plastic flow of material (Eq. (5b)). The values of the microhardness H and the surface slope $\tan\varphi$ are taken from Madhusudana [6]. The values for conductivity $\bar{k}$ and surface roughness $\bar{\sigma}$ are harmonic means of the material properties. All results presented here are compared with Eq. (5b) as it is assumed that the contact surface is deformed plastically and plastic flow occurs.

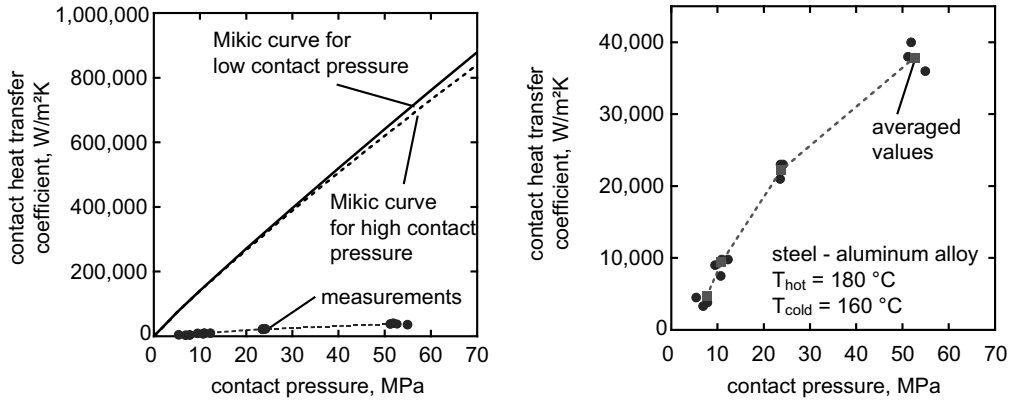

Fig. 9. Comparison of measurements and Mikić model, steel–aluminum combination. Left: full scale comparison. Right: zoom of the measurements.

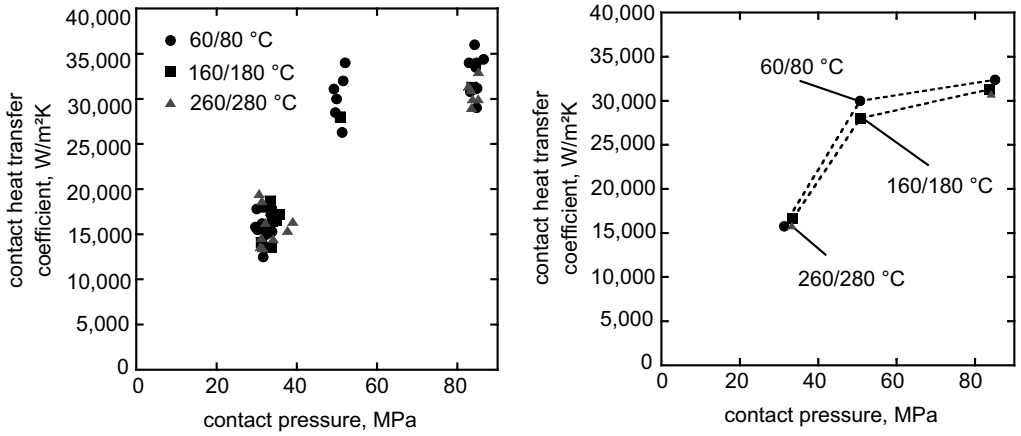

Fig. 10. Influence of the temperature on the contact conductance. Left: measurement data. Right: averaged values.

$$h_c = 1.13\frac{\tan\varphi\bar{k}}{\bar{\sigma}}\left(\frac{p}{H}\right)^{0.94} \quad \text{low pressure} \tag{5a}$$

$$h_c = 1.13\frac{\tan\varphi\bar{k}}{\bar{\sigma}}\left(\frac{p}{p+H}\right)^{0.94} \quad \text{high pressure} \tag{5b}$$

A comparison of the extrapolated Mikic curve and the measured data is shown in Fig. 9.

The contact conductance increases with pressure, but is clearly below the predicted values. The increase does not correspond to an exponent of 0.94 as suggested by Mikić, Eqs. (5b) and (5a). Instead, the contact heat transfer coefficient corresponds to an exponent of about 1 which is slightly above. The pressure dependence of the contact conductance is thus almost linear. Only the amplitude factor is much smaller compared to the existing model. Recent experimental data for contact conductance under cryogenic conditions [11] showed the same overestimation of the results compared to the Mikic models, Eqs. (5a) and (5b).

4.3. Temperature influence on the contact resistance

Next to the pressure influence on the heat transfer coefficient, the thermo-physical properties and thus the body temperatures may influence the contact heat transfer. To examine this influence, three different sets of initial body temperatures: 60/80 °C, 160/180 °C and 260/280 °C were investigated. Fig. 10 shows the result for a steel–steel combination for different pressures and temperatures.

Even if the standard deviation for the measurements is high, the influence of the temperature is not distinguishable and the values are close together. Higher temperatures above 500 °C allow the crystal microstructure of the materials to change. In this case an effect might be visible and should be investigated in further research to find a definite answer to that question.

5. Conclusions

A new method to measure thermal contact conductance is introduced. The time dependent temperature field of the surfaces of two body in contact are recorded with an infrared thermography camera. The resulting temperature data are the input for the solution of the related inverse heat conduction problem and yield the boundary heat flux at the contact interface. Together with the temperature jump at the interface the contact heat transfer coefficient is eval-

uated. The inverse problem is solved by the sequential estimation method considering future time steps to stabilise the solution and to reduce the time step size. First tests are performed with a steel–steel and a steel–aluminum alloy combination. The contact pressures vary from 7.5 to 85 MPa and the initial temperatures are between 60 °C and 280 °C. The results show an almost linear dependency of the contact heat transfer coefficient from the contact pressure, whereas the temperature influence for the investigated temperature range seems to be negligible.

6. Outlook

Further research should give more insight into the temperature influence, especially for higher temperatures. Although there is no direct influence of the temperature on the contact conductance, the decrease in hardness of the bodies due to high temperatures might be in the same order of magnitude as the values of the applied load and result in plastic flow and further contact spots compared to low temperature experiments.

The inverse method used at the moment is based on an analytical solution of a pure heat conduction problem. The heat losses due to radiation and natural convection of the test bodies are not considered yet. Therefore, the error in the IHCP algorithm is increased especially with increasing influence of radiation. To include these side effects in the calculation of the heat transfer coefficient, another inverse method is tested, the conjugate gradient method [1]. Here, the heat transfer coefficient is directly calculated from an optimisation between the measured and a calculated temperatures based on the results of the adjoint and sensitivity problems of the partial differential energy equation.

Acknowledgements

The authors acknowledge with thanks the support of the Federal Ministry of Economics and Technology, Germany and the Arbeitsgemeinschaft industrieller Forschung (AiF), Germany.

References

[1] O.M. Alifanov, Inverse Heat Transfer Problems, Springer, New York, 1994.
[2] J.V. Beck, K. Arnold, Parameter Estimation in Engineering and Science, Wiley, New York, 1977.
[3] J.V. Beck, B. Blackwell, C.R. St. Clair, Inverse Heat Conduction. Ill-Posed Problems, Wiley-Verlag, New York, 1985.
[4] H.S. Carslaw, J.C. Jaeger, Conduction of Heat in Solids, Oxford University Press, Amen House, London E.C.H, 1959.
[5] H. Fenech, W.M. Rosenhow, Prediction of thermal contact conductance of metallic surfaces in contact, ASME J. Heat Transfer (1963) 15–24.
[6] C.V. Madhusudana, Thermal Contact Conductance, Springer, New York, 1996.
[7] T.H. McWaid, E. Marschall, Thermal contact resistance across pressed metal contacts in a vacuum environment, Int. J. Heat Mass Transfer 35 (11) (1992) 2911–2920.
[8] B.B. Mikić, Thermal contact conductance: theoretical considerations, Int. J. Heat Mass Transfer 17 (1974) 205–214.
[9] C. Le Niliot, P. Gallet, Inverse heat conduction problems: recovery of heat line sources and boundary conditions, Rev. Gen. Therm. 37 (1998) 629–643.
[10] W.J. Parker, W.J. Jenkins, C.P. Butler, G.L. Abbott, Flash method of determining thermal diffusivity, heat capacity and thermal conductivity, J. Appl. Phys. 32 (1961) 1679–1684.
[11] R. Xu, H. Feng, L. Zhao, L. Xu, Experimental investigation of thermal contact conductance at low temperature based on fractal description, Int. Commun. Heat Mass Transfer 33 (7) (2006) 811–818.